European Journal of Wood and Wood Products (2026) 84:34
https://doi.org/10.1007/s00107-026-02388-3

Multi-parametric high-resolution MRI for the characterisation of water and PEG solutions in wood

Elisa Villani[1] · Valeria Stagno[1,2] · Alessandra Maiuro[2,3] · Genny Travisano[4] · Silvia Capuani[2,5]

Received: 3 October 2025 / Accepted: 19 January 2026

Abstract

Waterlogged wooden artifacts are often unstable when exposed to open air, and impregnation with polyethylene glycol (PEG) remains one of the most widely adopted conservation methods to ensure their long-term stability. Despite its widespread use, relatively few studies have focused on the interaction between PEG, water and wood. Motivated by the development and testing of new NMR-based imaging (MRI) protocols for analysing water-PEG-wood systems, NMR diffusion and relaxation experiments were first conducted on PEG-water solutions at increasing concentrations. High-field (9.4T) micro-MRI (μ-MRI) was then employed to examine the penetration and interaction of these solutions within chestnut wood, adapting diffusion models originally developed for medical diagnostics. NMR spectroscopy revealed clear concentration-dependent variations in relaxation and diffusion parameters, indicating a progressive reduction in molecular mobility with increasing PEG content. High-resolution μ-MRI weighted by T_2*, T_2, T_1, and diffusion (quantifying the diffusion coefficient D and the kurtosis parameter K) allowed non-destructive observation of the wood microstructure and the quantification of relaxation (T_2, T_1) and diffusion (D, K) values in the earlywood and latewood regions during treatment. Increasing PEG concentration resulted in decreasing T_1 and D values, while T_2 and K exhibited contrasting behaviors associated with changes in local molecular dynamics and microstructural heterogeneity. Notably, the kurtosis parameter proved sensitive to microstructural differences between earlywood and latewood and to the progressive evolution of the system during treatment. Overall, the study suggests the potential of μ-MRI approach to capture the increasing complexity of the water-PEG-wood system, supporting its applicability for non-invasive monitoring of consolidation treatments in small samples of waterlogged archaeological wood.

1 Introduction

In recent decades, nuclear magnetic resonance (NMR) techniques have emerged as a valuable diagnostic tool in the field of cultural heritage conservation (Proietti et al. 2018; Rehorn and Blümich 2018; Wagner et al. 2023). These methods have shown significant potential for analysing complex, multiscale materials such as waterlogged archaeological wood, which are often found in severely degraded conditions (Capuani et al. 2020; Stagno et al. 2021, 2024). NMR techniques can differentiate between bound and free water states in wood, providing insights into physical confinement and chemical composition in hardwoods and softwoods (Bardet et al. 2012; Gao et al. 2015; Li and Ma 2021, 2022). Since water dynamics often reflect alterations in porosity, cell wall integrity and the presence of degradation, the information obtained from NMR measurements is particularly relevant for conservation diagnostics. In submerged archaeological contexts, wooden artifacts are prone to chemical

✉ Elisa Villani
elisa.villani@uniroma1.it

[1] Department of Earth Sciences, Sapienza University of Rome, P.le Aldo Moro 5, 00185 Rome, Italy

[2] National Research Council Institute for Complex Systems (CNR-ISC), Physics Dpt., Sapienza University of Rome, P. le Aldo Moro 5, 00185 Rome, Italy

[3] Santa Lucia Foundation, IRCCS, Via Ardeatina 306, 00179 Rome, Italy

[4] Department of Environmental Biology, Sapienza University of Rome, P.le Aldo Moro 5, 00185 Rome, Italy

[5] National Institute for Nuclear Physics (INFN), Rome 1, Sapienza, Rome, Italy

Published online: 04 March 2026

and physical deterioration. Once exposed to open air, they may undergo structural collapse due to contractive capillary forces acting on the cell walls and shrinkage caused by the loss of bound water (Christensen et al. 2006; Stelzner et al. 2022). To guarantee wood's dimensional stabilisation and prevent collapse, polymers are frequently used to fill internal cavities via a moderate diffusion process. Historically, impregnation with polyethylene glycol (PEG) has been the most widely applied method for waterlogged wood treatment. Generally, low molecular weight PEG is suited for less degraded specimens while higher molecular weight PEG provides structural reinforcement in heavily deteriorated wood (Han et al. 2022; Stamm 1964; Villani et al. 2025). Assessing the state of preservation and the dynamics of impregnation is essential for evaluating the efficacy of conservation treatments and Magnetic Resonance Imaging (MRI) offers a promising non-invasive approach, enabling the visualisation of wood microstructure and the spatial distribution of consolidants within waterlogged wood (Cole-Hamilton 1995; Kanazawa et al. 2017a; Kowalczuk et al. 2019; Mori et al. 2021; Stagno et al. 2023). Previous MRI studies have demonstrated that relaxation and contrast-based imaging can detect changes induced by PEG impregnation. In particular, Kanazawa et al. 2017a reported a progressive decrease in longitudinal relaxation times (T_1) with increasing PEG and trehalose concentrations, interpreted as a consequence of reduced mobility and increased correlation times in viscous, polymer-rich environments. These results indicate that T_1 represents a robust parameter for monitoring the dynamics during consolidation treatments. In contrast, the behaviour of transverse relaxation T_2 has proven more difficult to interpret due to limited and ambiguous variations of its value across the treatment. Alternative contrast mechanisms have been explored by (Kanazawa et al. 2017b) applying Magnetization Transfer (MT) MRI, demonstrating a relatively uniform PEG penetration in small wood specimens but an insufficient impregnation in the inner regions of larger samples, even when high PEG concentrations were used. This approach proved effective for assessing sample-size-dependent impregnation efficiency but highlighted that MT contrast only provides an indirect and non-specific measure of macromolecular content and offers limited insight into water dynamics and microstructural confinement. More recently, (Mori et al. 2021) used 3D ultrashort echo time (UTE) MRI to reconstruct the spatial distribution of PEG in treated wood relying on the correlation between MRI signal intensity and increased PEG concentration.

Despite these advances, most NMR and MRI studies on treated wood remain primarily focused on qualitative or indirect visualisation of consolidant distribution. Moreover, MRI images are often limited by insufficient spatial resolution and by the difficulty of clearly relating image contrast to the water-PEG-wood interactions within different wood structures. MRI-based relaxation studies (Kanazawa et al. 2017a, b; Mori et al. 2021) and measurement of average translational self-diffusion coefficients obtained by pulsed-gradient NMR methods (Kowalczuk et al. 2019) do not provide spatially resolved information on diffusion processes and are generally interpreted within Gaussian diffusion framework. As a consequence, the microstructural heterogeneity of wood and the presence of restricted and non-Gaussian diffusion regimes associated with consolidant impregnation remain insufficiently characterised. Therefore, there is still a lack of adequate research focused on developing non-invasive MRI strategies capable of quantitatively characterising both molecular mobility and microstructural complexity during wood consolidation treatments. In this work, we drew inspiration from diffusion MRI models and experimental protocols originally developed in clinical research for medical diagnostics (De Santis et al. 2011; Jensen et al. 2005; Maiuro et al. 2025), in particular diffusion kurtosis imaging (DKI), which extends conventional diffusion MRI by quantifying deviations from Gaussian diffusion that are especially relevant in porous and heterogeneous materials. These approaches are here adapted to the specific physical and structural characteristics of wood.

In this framework, the study applies selected protocols to the investigation of a chestnut wood sample, combining NMR spectroscopy and multiparametric micro-imaging NMR (μ-MRI) to characterise PEG-water solutions at increasing concentrations and monitor their penetration into waterlogged wood. By quantifying relaxation and diffusion parameters and mapping their spatial distribution across the sample, we provide a non-destructive means to investigate conservation treatment and the evolving interactions between water, PEG and wood microstructure.

2 Materials and methods

2.1 Materials

Sweet chestnut (*Castanea sativa* Mill.), a species belonging to the Fagaceae family, is a ring-porous hardwood, characterised by large earlywood vessels arranged in distinct growth rings. These vessels often display an oblique to dendritic orientation, contributing significantly to the wood's structural and functional properties (Schweingruber 2007). In this study, a waterlogged chestnut wood sample with initial dimensions of approximately $1.0 \times 0.7 \times 0.8$ cm³ was first scanned and then sectioned into two subsamples ($1.0 \times 0.7 \times 0.4$ cm³). Sample C1 underwent stepwise impregnation treatment, while the other one was preserved as an untreated reference in its original waterlogged state.

Polyethylene glycol (MW 400), provided by Andrea Gallo S.r.l., was selected due to its low molecular weight, allowing an easy penetration into well-preserved wood such as in our case. Polyethylene glycol (PEG) is a linear polyether with the general formula $HO–(CH_2CH_2O)_n–H$, where n represents the number of ethylene oxide units. The average molecular weight of PEG used in this study is approximately 400 g/mol, corresponding to about 8–9 repeating units (Derkaoui et al. 2007). The treatment consisted of immersing the already fully water saturated C1 sample in distilled water - PEG 400 solutions at progressively increasing concentrations of 10%, 30% and 50% w/w, with each step lasting two weeks. This stepwise approach was used to enable gradual penetration of the consolidant, as commonly adopted in conservation practice (Christensen et al. 2012; Hoffmann 1986; Nguyen et al. 2018). Between acquisitions, C1 was stored in a controlled environment (25 ± 1 °C, 50% RH) to minimise variability and optimise treatment conditions.

Figure 1 summarises the experimental workflow applied in this study, including sample preparation, sequential treatment steps, and the NMR/MRI analysis pipelines for both solution and wood sample.

2.2 ^{1}H NMR spectroscopy, relaxation and diffusion of PEG-water solutions

Since PEG water interactions can significantly influence MRI contrast (Callaghan 1991; Kanazawa et al. 2017a), a preliminary characterisation of the relaxation and diffusion properties of the solutions was conducted to support the subsequent µ-MRI experiments. ^{1}H NMR measurements were performed on 700 µL of the prepared PEG–water solutions and on PEG 400 alone using a Bruker-Avance 400 MHz (9.4 T) spectrometer. The temperature during the experimental time was 296 K. Data acquisition and manual resonance peak integration were carried out using TopSpin® 2.0, while curve fitting was conducted using Origin® 8.5.

NMR spectra were obtained using a standard *zg* (zero-gradient) sequence, consisting of a single 90° radiofrequency (RF) excitation pulse followed by free induction decay (FID) acquisition. The RF pulse duration was 10 µs, with a recycle delay of 6 s, 2 scans (NS), an offset frequency of 1500 Hz, and a spectral width of 6 ppm. Relaxation and diffusion experiments were conducted to quantify T_1, T_2 and the molecular diffusion coefficient D. Transverse relaxation times (T_2) were determined using the Carr-Purcell-Meiboom-Gill (CPMG) sequence with 228 echo times (1–455 ms, 2 ms step), an interpulse delay of 500 µs, a repetition time (T_R) of 5 s and 8 scans per point. Longitudinal relaxation times (T_1) were obtained using an Inversion Recovery (IR) sequence with a recycle delay of 10 s, 16 inversion times (10–12000 ms) and 16 scans per point. Molecular diffusion coefficients (D) were measured using a Pulsed Gradient Stimulated Echo (PGSTE) sequence, with $\delta = 5$ ms, $\Delta = 80$ ms, 16 gradient steps and 16 scans per point. The magnetic field gradient was applied along the x-axis, orthogonal to the sample's longitudinal direction.

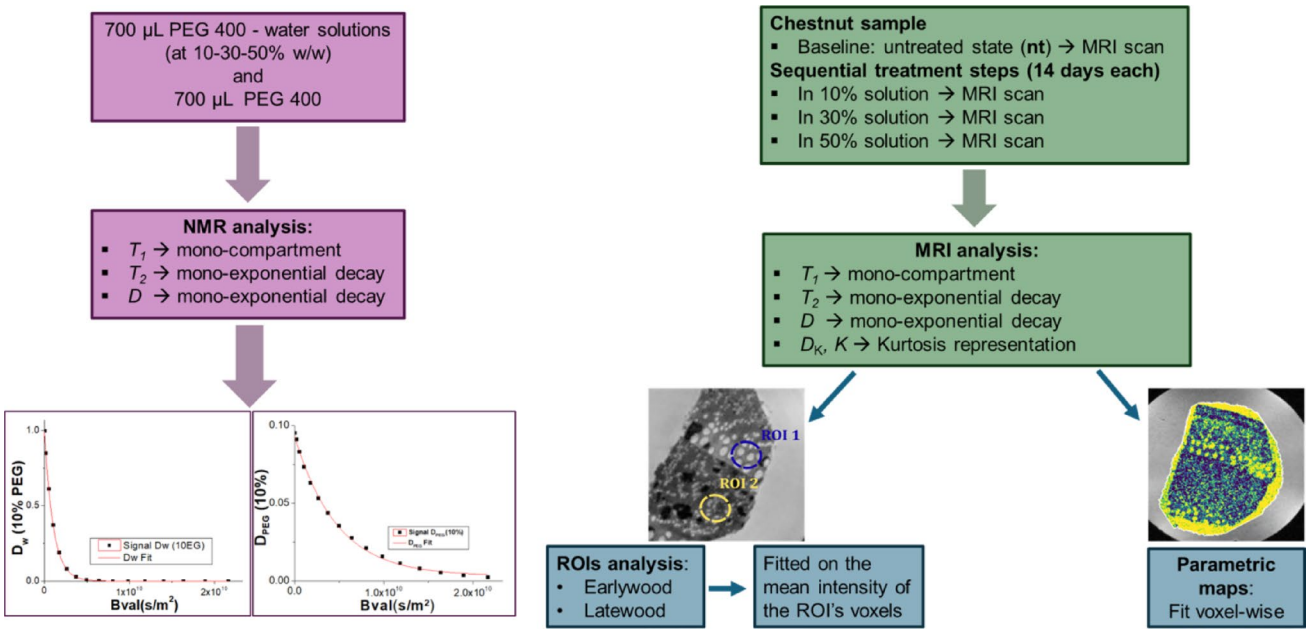

Fig. 1 Summary of the methodological workflow applied in this study, illustrating sample preparation, treatment steps, and the corresponding NMR and MRI analytical procedures

2.3 Multiparametric µ-MRI of wood

Before investigating the behaviour of PEG–water solutions within the wood matrix, µ-MRI was first performed on the chestnut sample in its entirety to analyse its untreated condition. Following this initial acquisition, sample C1 was then scanned after each treatment step. All µ-MRI acquisitions were performed on the same specimen throughout the impregnation stages to minimise anatomical variability and ensure that observed changes were solely attributable to the interaction between PEG and the wood-water system. This approach allowed for a direct comparison within specific anatomical regions. Spatially resolved images were acquired using a Bruker-Avance 400 MHz (9.4 T) spectrometer, equipped with 10 mm microimaging and high-performance gradient coils capable of producing magnetic field gradients up to 1200 mT/m with a rise time of 100 µs. Data acquisition and processing were carried out using ParaVision® 3.2 software. Samples were placed in 10 mm NMR tubes, either in distilled water or in their treatment solution (10–30-50% PEG) and set temperature was about 296 K.

The imaging protocol included the acquisition of T_2*-, T_2-, T_1-, and diffusion-weighted (DW) images, each optimised to highlight specific contrast mechanisms, with the aim of minimising imaging artifacts and maximising the signal-to-noise ratio (SNR) of the images. In NMR imaging, different image contrasts provide complementary information about the state of water in wood. T_1-w images primarily reflect the ease with which water molecules exchange energy with their surroundings and thus provide information about water mobility and its interaction with the wood-PEG matrix. T_2-w images are sensitive to the strength with which water is confined within the wood microstructure, allowing the distinction between water that moves more freely (white/light pixels) and water tightly associated with cell walls (gray/black pixels). Diffusion-weighted images investigate the ease with which bulk water can move through wood, providing information on pore connectivity and how PEG treatment affects water transport pathways. Applied sequences are listed below and detailed parameters are provided in Table 1.

- T_2*-w images were collected using a FLASH (Fast Low Angle Shot) sequence;
- T_2-w images were acquired using a MSME (Multi Slice Multi Echo) sequence with 16 echo times ranging from 14.3 to 228.5 ms, to measure T_2;
- T_1-w images were acquired with an IR-EPI (Inversion Recovery Echo Planar Imaging) with 16 inversion times ranging from 15 to 4000 ms (step 185 ms) to measure T_1;
- DW images were collected using a DW-EPI sequence, with 7 effective b-values (352, 785, 1081, 1487, 2122, 2610, 3088 s/mm²), with $\Delta = 40$ ms and $\delta = 2$ ms to quantify diffusion coefficient D and the kurtosis parameter K.

Table 1 Acquisition parameters used in applied MRI sequences

Sequence	TE (ms)	TR (ms)	FOV (mm²)	STK (mm)	MTX (px)
FLASH	3.7	1000	13 × 13	0.3	256 × 256
MSME	14.3	2000	13 × 13	0.3	256 × 256
IR-EPI	36	4000	13 × 13	0.3	256 × 256
DW-EPI	27.8	3000	10 × 10	0.6	128 × 128

TE is the echo time, TR the repetition time, FOV is the field of view, STK the thickness of chosen slice, MTX the size of the matrix

The acquisition parameters reported in Table 1 are a compromise between the limited possibilities of values offered by the hardware and software of the MRI scanner and the optimisation of the signal to noise ratio (SNR) and image contrast to obtain good quality images from bulk water (Capuani et al. 2020; Stagno et al. 2023). Regions of interest (ROIs) were selected based on structural features visible in T_2*-w images. Two key circular ROIs, with a diameter of 0.9 mm, were defined: ROI 1 from the earlywood region mainly containing larger vessels, ROI 2 from the latewood region with smaller lumen cells (Fig. 2).

Quantitative analysis of signal evolution in these ROIs was performed using mono-exponential fitting models using Origin® 8.5 on the mean of the ROIs' voxels. The following equations were used to extract relaxation and diffusion parameters:

- For T_2 estimation,

$$S(t) = S_0 \exp\left(-t / T_2\right) + c \quad (1)$$

where S(t) is the signal intensity at echo time (t), S_0 is the initial signal at $t = 0$, T_2 describes the decay of transverse magnetisation due to spin–spin interactions, and c is a constant offset accounting for baseline noise.

- For T_1 estimation,

$$S(t) = S_0 \left[1 - 2\exp\left(-t / T_1\right)\right] \quad (2)$$

where S(t) is the signal intensity measured at inversion time t, S_0 is the maximum signal intensity after full longitudinal relaxation, T_1 represents the recovery of longitudinal magnetisation due to spin-lattice interactions.

- For Diffusion coefficient estimation,

$$S(b) = S_0 exp(-bD) + c \quad (3)$$

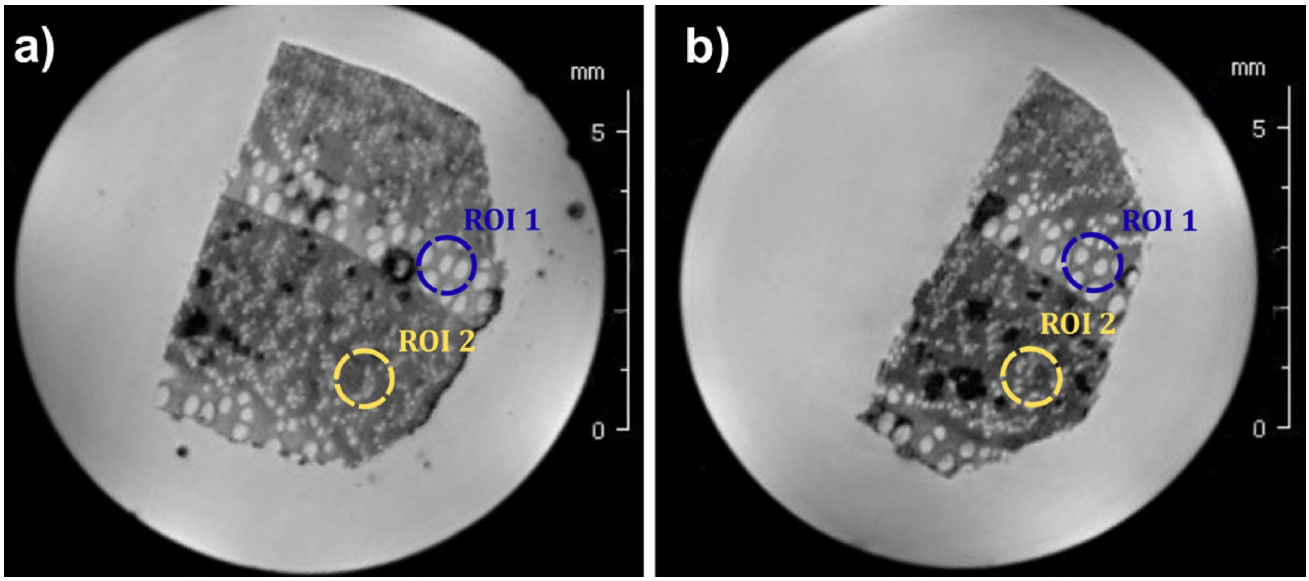

Fig. 2 T_2*-w images of untreated (**a**) and 10% PEG-treated (**b**) samples. ROIs are marked as follows: dark blue = earlywood (ROI 1), yellow = latewood (ROI 2). The diameter of these regions is about 0.9 mm

where S(b) is the signal intensity measured at a given b-value, S_0 is the signal intensity at $t=0$, D is the apparent diffusion coefficient (m^2/s) and b is calculated as:

$$b = \gamma^2 \cdot g^2 \cdot \delta^2 \cdot (\Delta - \delta/3) \quad (4)$$

where, γ is the gyromagnetic ratio of the proton (2.675×10^8 $rad \cdot s^{-1} \cdot T^{-1}$), g is the gradient strength (T/m), δ is the gradient duration (s), Δ is the diffusion time (s).

The diffusion coefficient D extracted from a mono-exponential fit quantifies the average rate at which water molecules (or water and PEG molecules) move through wood's porous structure. It reflects how easily water penetrates and diffuse through the interconnected pores and cell walls of the wood (Anisimov et al. 1998). To further investigate the interaction between solutions and wood structures, we applied the Kurtosis representation (Jensen et al. 2005), an approach that has proven to be more sensitive and specific in medical diagnostics than the classical mono-exponential diffusion decay (Maiuro et al. 2025). Therefore, in addition to the mono-exponential fit, we also performed the Kurtosis fit:

$$S(b) = S_0 \exp\left(-bD_K + \frac{1}{6}K(bD_K)^2\right) \quad (5)$$

where D_K is the apparent diffusion coefficient (m^2/s) and K is the kurtosis parameter whose values might account for non-Gaussian diffusion as follows:

- $K \approx 0$: indicates Gaussian diffusion. In this case, the system is well described by D obtained using the mono-exponential fit.
- $K > 0$: indicates non-Gaussian diffusion and the presence of membranes and microstructures that hinder and restrain water diffusion.

The K values may highlight interesting new information about the wood structure itself, pinpointing regions with higher complexity and chaotic arrangements or enhancing the edges of the wood's microstructures.

The initial values for each fitting procedure were established as follows: S_0 was initialised considering the intensity of the highest point, T_1 was set at 1000 ms, T_2 at 20 ms, D at 2.1 E-9 (m^2/s), D_K at 2.1 E-9 (m^2/s) and K at 0. The quality of the fits was assessed by the coefficient of determination (R^2).

Additionally, to better show the spatial distribution of T_2 and D parameters across the entire sample, parametric maps were obtained using a custom Python script performing a voxel-wise nonlinear least-squares algorithm. DW images were denoised performing the Patch2Self algorithm from dipy library (dipy.org) (Fadnavis et al. 2022).

3 Results and discussion

3.1 ^{1}H NMR spectroscopy, relaxation and diffusion of PEG-water solutions

The ^{1}H NMR spectra of aqueous PEG 400 solutions at different concentrations are shown in Fig. 3. In the 10%

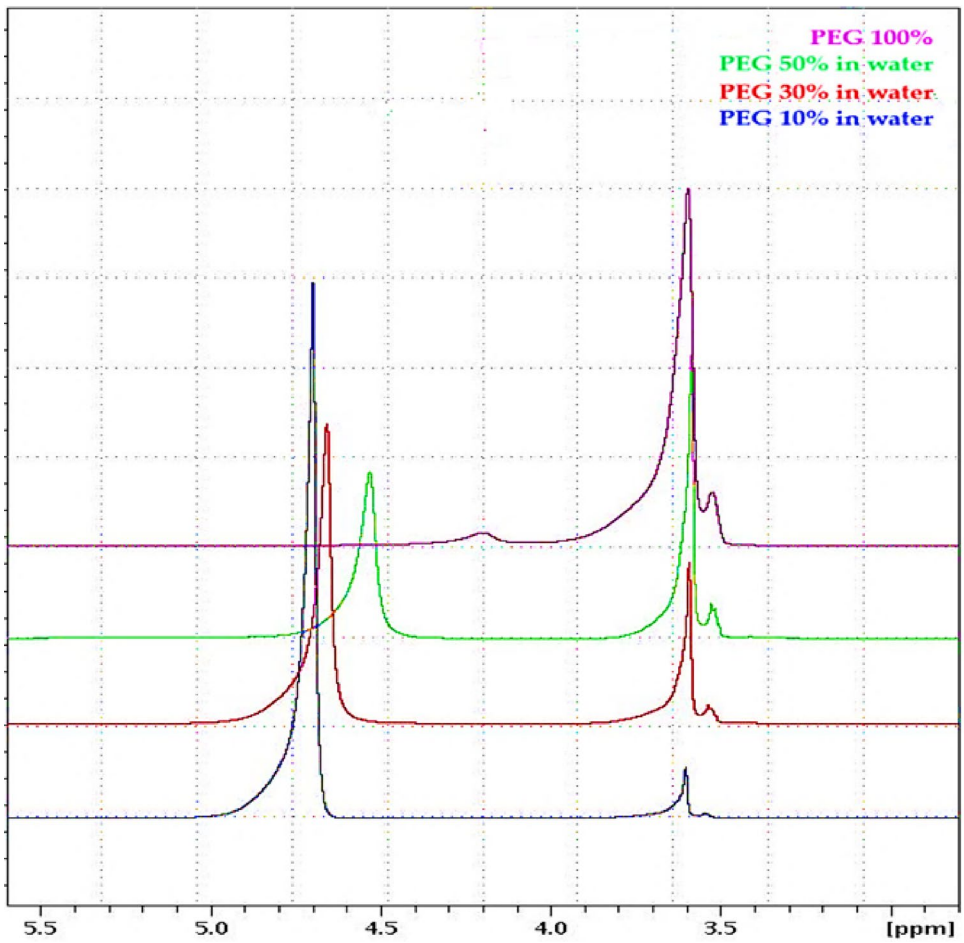

Fig. 3 ^{1}H NMR spectra of PEG 400 in water at various concentrations: 10% (blue), 30% (red), 50% (green) and pure PEG 400 (violet) obtained at 9.4T. The water resonance appears at 4.7 ppm in the 10% solution and gradually shifts downfield (to 4.6–4.5 ppm) in more concentrated solutions, where it overlaps with the PEG terminal hydroxyl group which is otherwise visible at 4.3 ppm in the violet spectrum. The intense peak resonance at 3.62 ppm corresponds to the methylene protons of the PEG backbone with a shoulder at about 3.52 ppm attributed to the terminal -CH_2-OH groups. For visual clarity, spectra were overlaid during post-processing, therefore the y-axis, reporting relative signal intensities in arbitrary units, has been omitted

Table 2 T_1, T_2 and D values obtained for analysed solutions with errors deriving from fitting

PEG (%)	T_1 (ms)		T_2 (ms)		D (m^2/s)	
	T_{1W}	T_{1PEG}	T_{2W}	T_{2PEG}	D_W	D_{PEG}
10	2049 ± 190	790 ± 8	943 ± 75	574 ± 59	(9.7 ± 0.1) x 10^{-10}	(2.1 ± 0.1) x 10^{-10}
30	1518 ± 9	627 ± 4	95.7 ± 0.4	357 ± 9	(5.1 ± 0.1) x 10^{-10}	(6.9 ± 0.1) x 10^{-11}
50	798 ± 2	430 ± 2	62.0 ± 0.1	274 ± 3	(7.2 ± 0.1) x 10^{-10}	(8.6 ± 0.2) x 10^{-11}
100	-	414 ± 5	-	133 ± 1	-	(5.6 ± 0.1) x 10^{-11}

T_{1W}, T_{2W}, D_W refer to water resonance while T_{1PEG}, T_{2PEG}, D_{PEG} to methylene proton resonance of the polymer. Numbers 10-30-50-100 refer to PEG concentration (wt%)

PEG solution spectrum, the water resonance is centered at approximately 4.7 ppm while PEG-related resonances are observed between 3.5 and 3.7 ppm. The main signal at 3.62 ppm was assigned to the internal methylene protons (-CH_2CH_2O-), with a shoulder at 3.52 ppm corresponding to terminal -CH_2 groups. A broad hydroxyl group signal at around 4.2 ppm is visible in the pure PEG 400 spectrum and it is undetectable for the solutions due to fast proton exchange with water.

The chemical shift of the water resonance varies with PEG concentration, consistently with literature observations, moving from 4.7 ppm in dilute solutions to 4.5 ppm in more concentrated ones, likely due to exchange dynamics (Jora et al. 2016). Average values of the relaxation times (T_1 and T_2) and diffusion coefficients (D) measured for both the water signal and the PEG methylene (-CH_2-CH_2-O-) proton resonance are reported in Table 2.

For 100% PEG, only the methylene resonance was considered, with T_{1PEG} = 414 ± 5 ms and T_{2PEG} = 133 ± 1 ms. Concerning the solutions, the longitudinal relaxation times for both water (T_{1W}) and PEG methylene protons (T_{1PEG}) decrease progressively as PEG concentration increases, reflecting a reduced molecular mobility in increasingly viscous environment (Clop et al. 2012; Jora et al. 2016; Lüsse and Arnold 1996).

As shown in Table 2 for 10% PEG solution, T_{1W} value is significantly longer than T_{1PEG} (2049 ± 190 ms & 790 ± 8 ms respectively) reflecting the higher mobility of free or weakly

bound water compared to the polymer chains (Clop et al. 2012; Jora et al. 2016). As PEG concentration increases up to 50%, water becomes more involved in the polymer's hydration layer, leading to restricted dynamics, with a consequent T_1 reduction for both species.

A similar trend is observed for transverse relaxation times (T_2). At 10% PEG, $T_{2W} > T_{2PEG}$, indicating that water molecules experience higher mobility than more constrained PEG chains. However, as the concentration increases, T_{2W} decreases drastically, indicating stronger interactions with the polymer. In the pure PEG 400, T_{2PEG} has its minimum value.

Diffusion measurements (obtained with a diffusion time equal to $\Delta = 80$ ms) further confirm these observations. At 10% PEG, the diffusion coefficient of water (D_W) is already reduced relative to pure water, consistent with the occurrence of intermolecular interactions with PEG due to water hydration. As concentration increases, D_W continues to decrease, reflecting a growing restriction of water mobility and the priority role of PEG hydration by water. At 10%, D_{PEG} is around 2.0×10^{-10} (m^2/s), and the decrease in its values with increasing concentration is consistent with reduced chain mobility caused by inter-chain interactions. At a 50% concentration, a slight deviation from the decrease in the D value has been observed in both D_W and D_{PEG}. This phenomenon may result from structural rearrangements within the PEG chains, aligning with the transition toward a 'spread-gel' phase as reported in literature for PEG 400 aqueous solutions (Derkaoui et al. 2007). While further investigation is required to validate this hypothesis, such analysis goes beyond the scope of the current study and was not pursued in detail at this stage. Finally, at 100% PEG, D_{PEG} value reaches its minimum (about 5.6×10^{-11} m^2/s) as the system is dominated by the absence of solvent-mediated mobility.

3.2 Multiparametric µ-MRI

Axial T_2*-weighted images of the chestnut wood sample, acquired before and after impregnation (10 and 30% PEG), are shown in Fig. 4. In this orientation, the images provide a detailed visualisation of the wood cross-section, allowing the observation of its anatomical features and the clear distinction between earlywood and latewood regions. The combination of low paramagnetic iron impurity content and optimised imaging parameters enabled the acquisition of clear images with strong tissue contrast. Sample C1, being a contemporary well-preserved waterlogged specimen, appears structurally intact and free from microscopic degradation, which is in contrast frequently observed in archaeological wood (Stagno et al. 2023; Stagno and Capuani 2022). In general, the earlywood region in chestnut is characterised by large, evenly distributed vessels with wide lumina and thin walls, which appear as light voxels in the images. In contrast, the latewood region consists of smaller vessels (brighter spots) and partially oriented parenchyma cells and fibres with smaller cavities and thicker walls, resulting in a lower signal intensity and darker grey voxels.

The annual growth rings are distinctly visible, as well as localised dark areas likely corresponding to polyphenolic compounds or extractives, as previously reported by Stagno et al. (2024). Quantitative relaxation and diffusion values derived from selected ROIs, defined in corresponding MR images as described in Sect. 2.3, are reported with associated fitting errors in Table 3. In the untreated sample, T_1 values are relatively high in both regions ($T_{1EW} = 1332 \pm 190$ ms and $T_{1LW} = 1479 \pm 301$ ms) and progressively decrease with increasing PEG concentration, in agreement with T_1 values of PEG and water reported in Table 2.

Conversely, T_2 shows an opposite trend, with a gradual increase upon impregnation. This behaviour can be explained by observing the individual relaxation values of

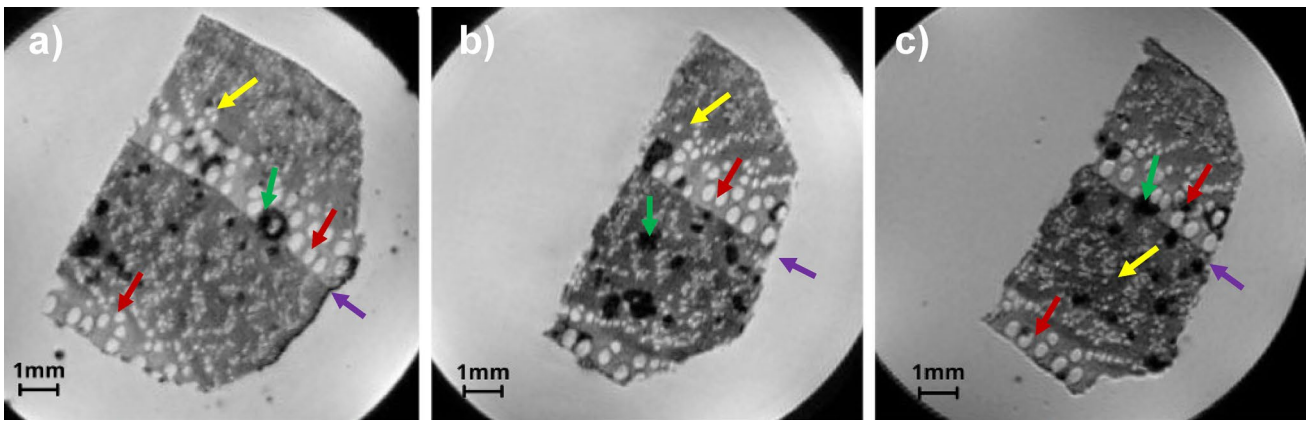

Fig. 4 T_2*-w images (STK 0.3 mm, in-plane resolution of 50×50 μm^2) of the chestnut sample, untreated (**a**) and treated with 10% and 30% PEG solutions (**b-c**) respectively. Arrows highlight important morphological features as the annual growth ring (violet), large earlywood vessels (red), small vessels and parenchyma cells in the latewood area (yellow) and polyphenolic extractives (green)

Table 3 T_1, T_2 and D values for selected ROIs in untreated (un.) and PEG-treated sample (10–30-50%)

ROI 1 (earlywood)				ROI 2 (latewood)			
	T_1 (ms)	T_2 (ms)	D (m^2/s)		T_1 (ms)	T_2 (ms)	D (m^2/s)
un.	1332±190	15.2±0.2	(1.6±0.1) x 10^{-9}	un.	1479±301	11.5±0.2	(1.3±0.1) x 10^{-9}
10%	1227±113	16.3±0.4	(1.5±0.1) x 10^{-9}	10%	1121±218	13.1±0.4	(1.0±0.1) x 10^{-9}
30%	621±94	41.3±1.7	(9.4±1.1) x 10^{-10}	30%	831±119	39.5±1.8	(7.9±1.2) x 10^{-10}
50%	311±33	85.7±2.8	(1.9±5.6) x 10^{-10}	50%	411±24	80.3±8.2	(6.4±13.8) x 10^{-10}

Diffusion values at 50% PEG exhibit large fitting errors due to chemical shift artefacts and are therefore not reliable; they are reported for indicative purposes only

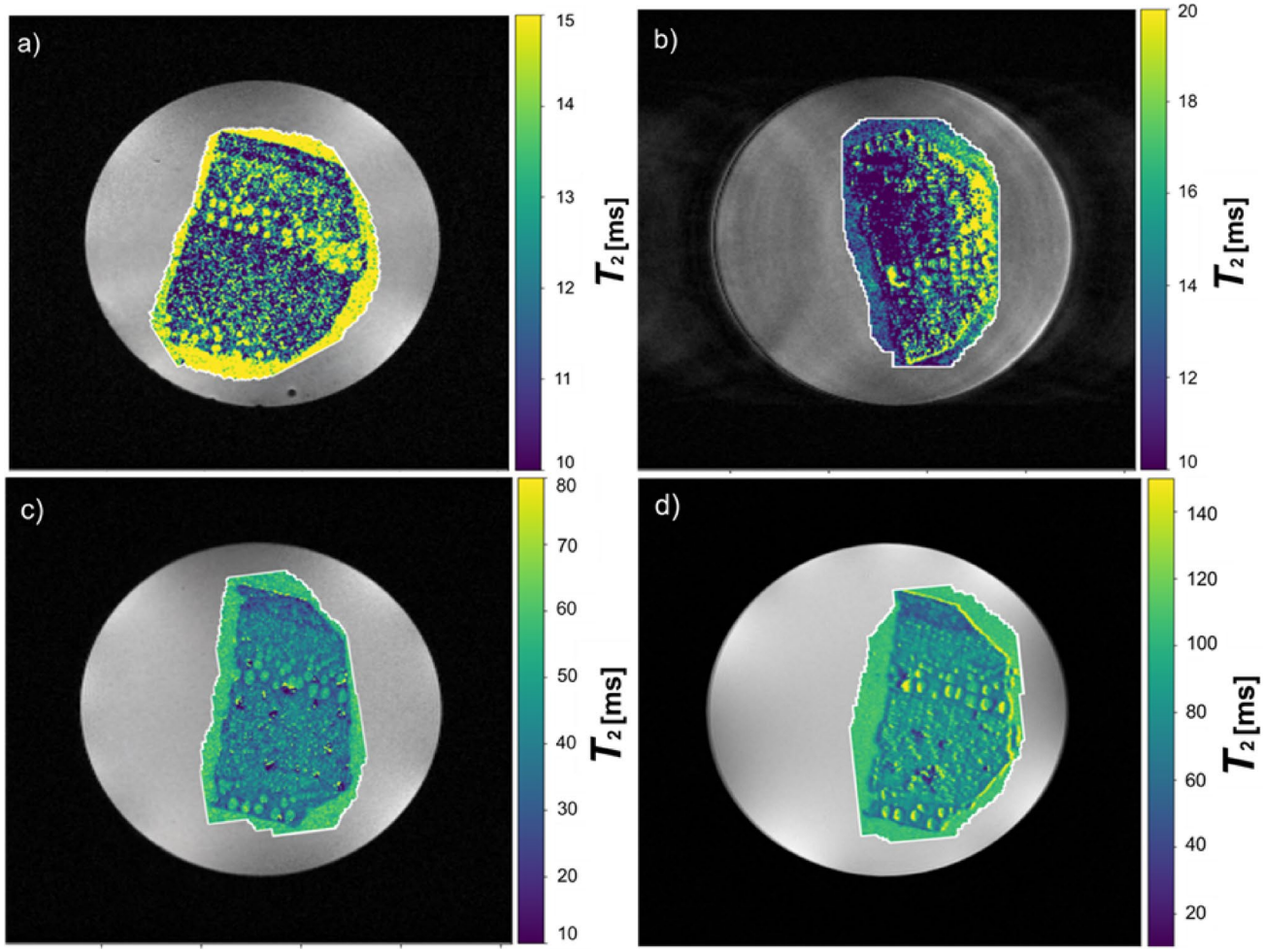

Fig. 5 T_2 maps (with STK of 0.3 mm and in-plane resolution of 50 × 50 µm^2) of wood samples: **a** untreated, **b**–**d** after treatment with PEG at 10%, 30%, and 50% concentration, respectively. The colour scale on the right of each image represents T_2 (ms), with warmer tones indicating higher values. In the untreated sample, the distribution of T_2 values is broader, reflecting heterogeneous water populations within the wood matrix. After treatment, a progressive increase and homogenisation of T_2 values is observed

water and PEG reported in Table 2 and considering that, in imaging mode, we quantify the average relaxation values of protons in solution. In particular, the reported values are obtained by averaging the signal over all pixels within the selected ROIs, thereby combining contributions from regions with longer and shorter transverse relaxation times. Additional insights are provided by the T_2 maps in Fig. 5, which enable a pixel-by-pixel visualisation across the entire sample.

In the untreated reference sample (Fig. 5a), yellow areas corresponding to T_2 values of approximately 15 ms are mainly located around the sample and inside vessels lumina, reflecting the presence of water population with higher mobility. Darker colour are mostly spread along latewood areas which in fact correspond to slightly smaller T_2 values.

These observations are consistent with studies reporting differences in spin-spin relaxation time for water residing in larger and less constrained vessels compared to water confined in smaller pores (Kowalczuk et al. 2019). Following PEG impregnation, the yellow zones progressively shift to green hues, indicating longer T_2 not only in the ground tissue but also within larger vessels. At 30% PEG, T_2 values in the map range from ~20–30 ms in fibres and ground tissue to ~40–60 ms in vessel lumina, whereas at 50% PEG the entire sample shows extended T_2 values, in the range of 80–120 ms. These maps provided a spatial distribution of T_2 values in accordance with the quantitative trends observed for the single ROI-based analysis reported in Table 3 and allowed an extensive visualisation of the parameter behavior in the entire section of the sample.

The observed increase in transverse relaxation time can be attributed to a reduction of water-cell wall interactions induced by PEG uptake. Similar behaviour has been previously reported using higher molecular weight PEG and changes in T_2 were interpreted as resulting from both the redistribution of water among pores of different sizes and the occupation of hydrogen-bonding sites at the cell walls by consolidant molecules, limiting surface occupation and exchange processes (Bannister 1990). From a physical perspective, transverse relaxation in wood, in other porous materials or biomaterials as bones, is strongly influenced by magnetic susceptibility differences between the solid matrix and the pore fluid. As example, in biomaterials such as spongy cancellous bone, where water and bone marrow reside within the pores of a mineral matrix, the magnetic susceptibility difference between water and bone mineral is about 1 ppm, while that between bone marrow and bone is approximately 0.4 ppm. Variations in the relative amounts of these pore fluids, for example due to pathological conditions such as osteoporosis, are reflected in measurable changes in T_2 relaxation times (De Santis et al. 2010; Rebuzzi et al. 2013).

In the case of wood, water and PEG, water is more diamagnetic than wood, with a susceptibility mismatch of approximately 0.2–0.4 ppm. Considering PEG molecular structure, hydrophilicity, and density compared to wood, we can reasonably think that the magnetic susceptibility of PEG is greater than that of water and less than that of wood. If the difference in magnetic susceptibility between PEG and wood is smaller than that between water and wood, two concurrent effects likely contribute to prolong T_2. First, increasing polymer concentration reduces the susceptibility difference at the wood-wall-solution interface; this attenuates the internal dephasing gradients and increases transverse relaxation. Second, the overall relaxation rate is influenced by the increasing fraction of PEG molecules which from 30% concentration are characterised by longer T_2 values than water (see Table 2). The combination of these factors results in a progressive increase in the mean T_2 observed during the consolidation treatment as reflected by the ROI-based analysis (Table 3) and spatially resolved maps (Fig. 5).

Diffusion measurements highlight the confinement of water due to the wood's porous structure, with D values (Table 3) lower than those of free water and slightly higher in earlywood than in latewood, in agreement with the larger vessels cross-section. The reported diffusion coefficients represent an average measure of molecular mobility within investigated ROIs, reflecting the combined contribution of water and PEG protons under the chosen experimental conditions. After the first impregnation step, a reduction in D is observed in both regions, consistent with the replacement of pure water by more viscous water-PEG solutions. At higher concentrations (30–50% PEG), the acquired images are affected by chemical shift artefacts due to the coexistence of two proton pools with distinct resonances. Indeed, in diffusion-weighted imaging, when no frequency-selective excitation is applied, these signals overlap in the reconstructed images, leading to superimposed contributions from water and PEG protons. As a result, the effective image resolution decreases and it further affects ROI definition and quantitative map reconstruction, as visible in Fig. 6. This limitation will be addressed in future experiments by implementing selective signal suppression schemes and alternating acquisitions for the resonance of water and PEG (which differ of about 1.2 ppm), to clarify their individual diffusion behaviours and provide a more accurate characterisation of the impregnation process. Nevertheless, with increasing PEG concentrations, a general reduction of diffusivity is observed, which is consistent with the expected behaviour of confined water and its progressive replacement by PEG solutions (Kowalczuk et al. 2019).

The application of the Kurtosis representation shows interesting results as reported in Table 4, providing additional insights on water and solution pathways in wood microstructure. In the untreated sample, the K value in earlywood ($K \approx 0.6$) indicates a water diffusion regime which only slightly differs from Gaussian behaviour, while values in latewood ($K \approx 1.0$) reflect a more complex structure. Earlywood cell types (mainly vessels) are large in diameter with thin cell walls, while latewood cells mostly have smaller diameters with thicker walls. Wider lumina give earlywood areas a more open and porous structure that facilitates fluid transport. Latewood, instead, has narrower lumina and a higher proportion of solid material, imposing stronger restrictions. Our results therefore suggest that K is more sensitive to the abovementioned microstructural difference than D coefficient, while the diffusion coefficient provides an average measure of mobility, the kurtosis parameter

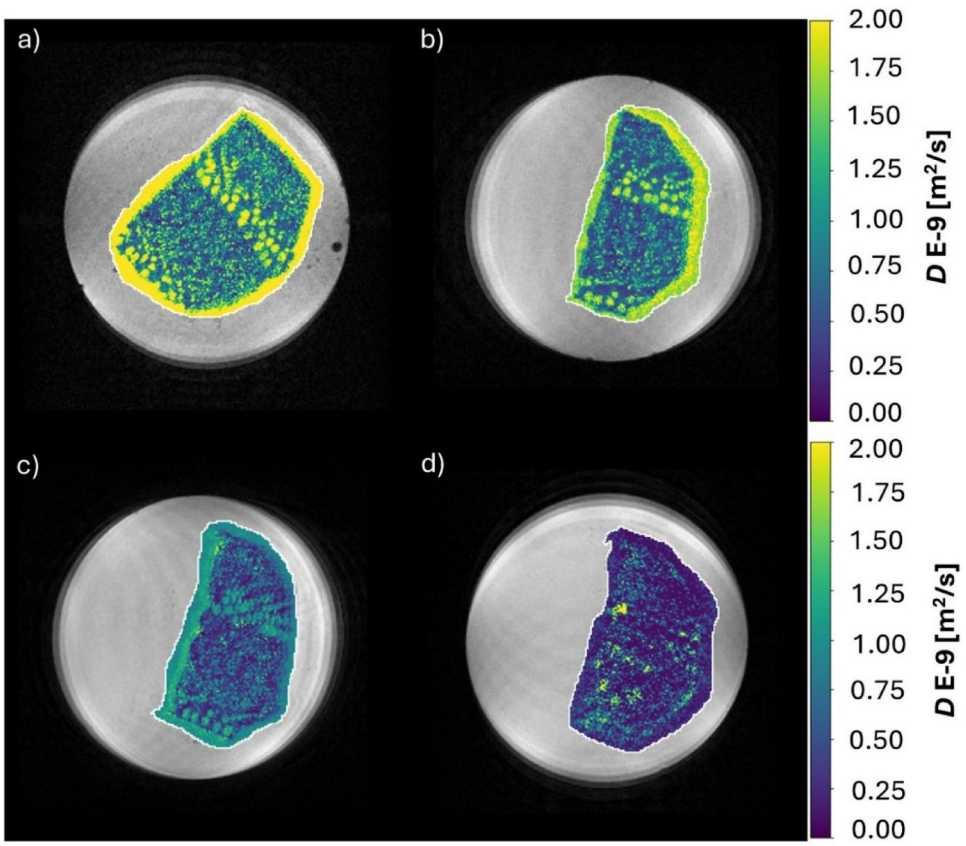

Fig. 6 Parametric maps (STK 0.6 mm, in-plane resolution of $78 \times 78\ \mu m^2$) of diffusion coefficient D of wood samples: **a** untreated, **b-d** after treatment with PEG at 10%, 30%, 50% concentration, respectively. The colour bar on the right represents D magnitude (m^2/s), with warmer colours indicating higher values. With increasing PEG concentration, a progressive reduction of the image resolution is observed mainly due to the chemical shift artifacts. Note that the maps at 50% PEG are affected by severe artefacts and that the derived D values are therefore associated with large uncertainties

Table 4 D_K and K values for selected ROIs in untreated (un.) and PEG treated sample (10–30-50%). In both ROIs, the values at 50% PEG exhibit fitting errors due to chemical shift artefacts in the acquired images and are reported for indicative purposes only

ROI 1 (earlywood)			ROI 2 (latewood)		
	D_K (m^2 /s)	K		D_K (m^2 /s)	K
un.	$(1.66 \pm 0.05) \times 10^{-9}$	0.59 ± 0.01	un.	$(0.98 \pm 0.04) \times 10^{-9}$	1.02 ± 0.02
10%	$(1.61 \pm 0.05) \times 10^{-9}$	0.60 ± 0.02	10%	$(0.89 \pm 0.10) \times 10^{-9}$	0.90 ± 0.08
30%	$(0.69 \pm 0.05) \times 10^{-9}$	1.22 ± 0.05	30%	$(0.52 \pm 0.04) \times 10^{-9}$	1.54 ± 0.07
50%	$(0.13 \pm 0.12) \times 10^{-9}$	1.70 ± 8.36	50%	$(0.20 \pm 0.21) \times 10^{-9}$	3.44 ± 1.81

complementarily captures deviations from Gaussian diffusion arising from microstructural heterogeneity and restriction. In addition, upon PEG impregnation, mean K values increase to values exceeding ~ 1.2–1.4 (Table 4) suggesting the emergence of compartments and microenvironments in which water is more restrained and characterised by a non-Gaussian motion propagator due to the interaction with PEG molecules and the wood's microstructure. The diffusion coefficient values obtained using the kurtosis representation applying Eq. 5 follow the trend previously observed for mono-exponential diffusion coefficient derived from Eq. 3 and are reported in Table 4.

In Fig. 7, the parametric non-Gaussian diffusion maps are displayed for each PEG percentage. The K map of the untreated wood (Fig. 7e) shows an average K value that is homogeneous across the entire sample, while the ones obtained for treated wood (Fig. 7f-h) reveal microstructural details, with higher K values particularly in earlywood pores characterised by water following a non-Gaussian motion. Overall, K highlights deviations from purely Gaussian diffusion, providing sensitivity to microstructural complexity. Higher K values may highlight restricted or heterogeneous water motion within the wood, emphasising structural differences such as denser latewood regions or the pore network in earlywood, where diffusion follows a non-Gaussian behaviour. The trends of all the estimated parameters as a function of the PEG concentration in the chestnut sample are summarised in Fig. 8. The behaviour of T_1 and D (Fig. 8a and c), evaluated through the mono-exponential fitting, decreases with increasing PEG concentration, indicating a progressive reduction of molecular mobility due to increased solution viscosity and confinement. This decrease is more pronounced in earlywood, consistently with larger lumen dimensions, suggesting higher sensitivity of its

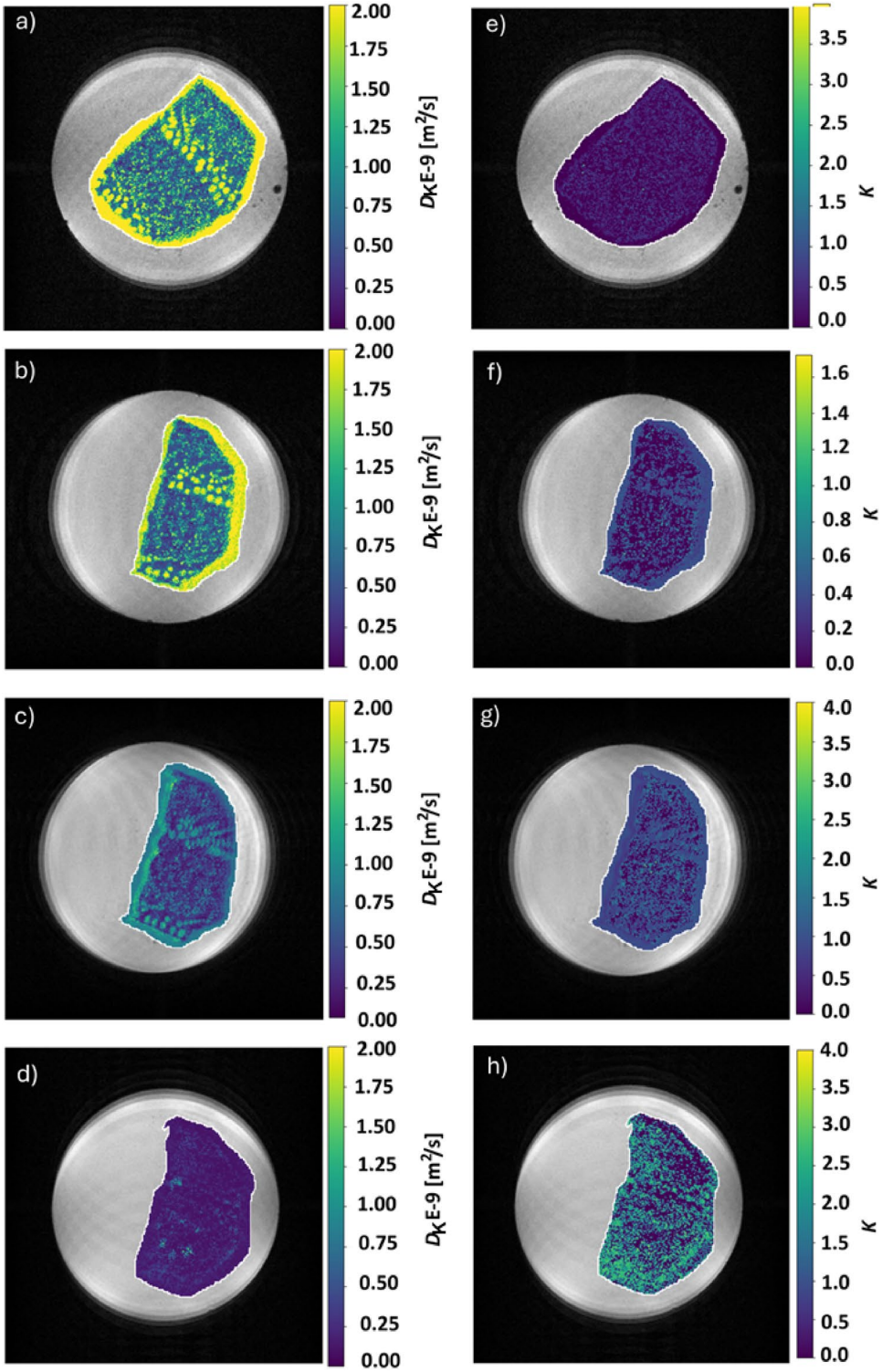

Fig. 7 Parametric maps of diffusion coefficient D_K (STK 0.6 mm, in-plane resolution of 78 × 78 μm^2) of wood sample: **a** untreated, **b-d** after impregnation with PEG at 10%, 30%, 50% concentration, respectively. Corresponding maps of the kurtosis parameter K: **e** untreated sample, **f-h** after treatment with PEG at 10%, 30%, 50% concentration, respectively. Colour bars indicate the magnitude of D (m²/s) and K, with warmer colours representing higher values. With increasing PEG concentration, a progressive reduction of the image resolution is observed, mainly due to the chemical shift artifact. Note that the maps at 50% PEG are affected by severe artefacts and that the derived D_K and K values are therefore associated with large uncertainties

microstructure to the treatment solution. Conversely, T_2 (Fig. 8b) increases at higher PEG concentrations (> 30%) in both regions, reflecting the combined relaxation contributions of water and PEG within the ROIs and the shielding effect of the PEG which reduces the magnetic susceptibility difference at the interface between water and wood, positioning itself right at the interface. The trend suggests, as previously discussed, a reduction of water–cell wall interactions due to PEG accumulation at pore cell-walls, resulting in prolonged relaxation times across the sample. The diffusion coefficients obtained either from conventional analysis (D) or from kurtosis fitting model (D_K, Fig. 8d)

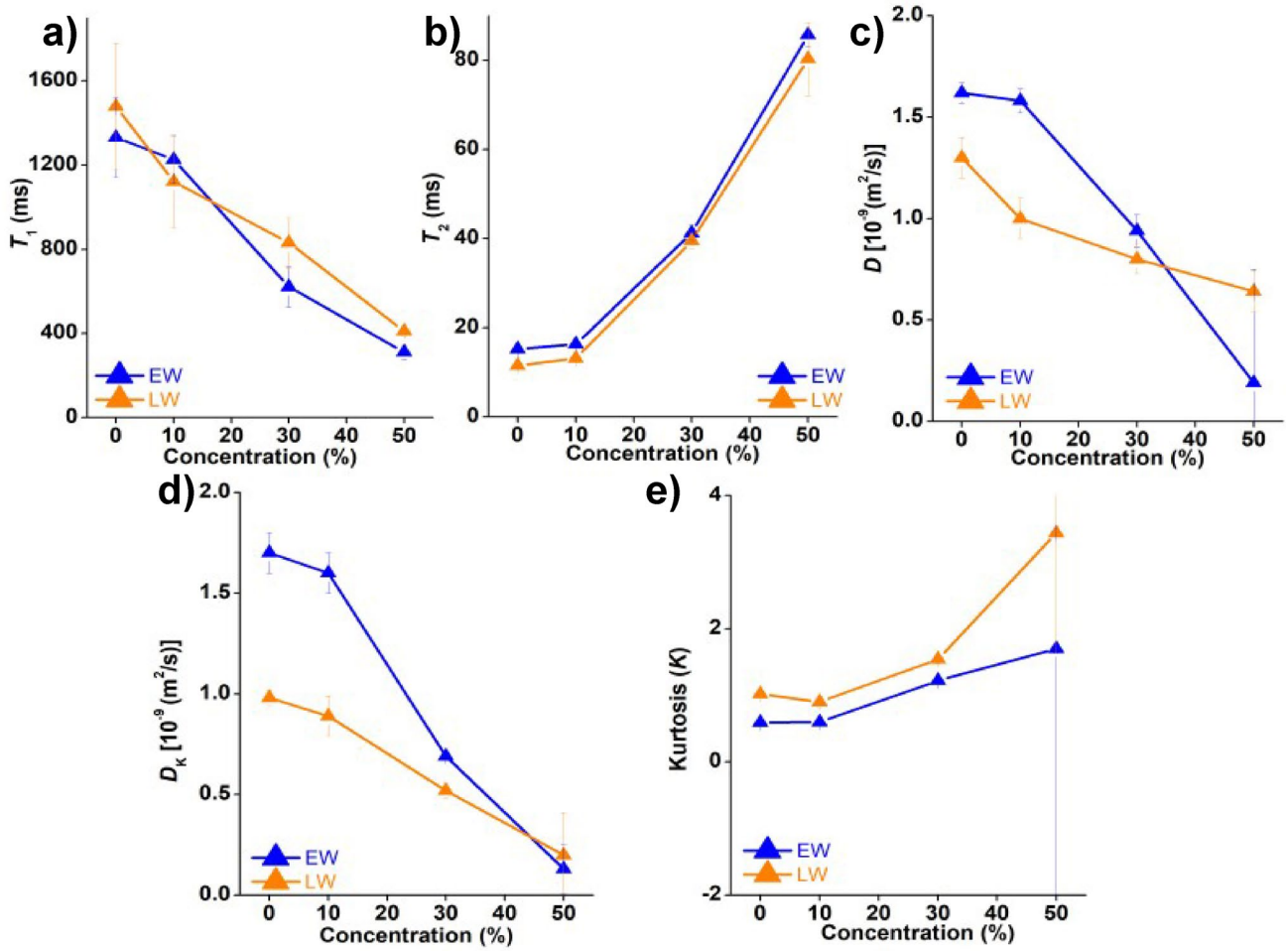

Fig. 8 Summary of the main trends of relaxation and diffusion parameters (T_1, T_2, D, D_K, and K) as a function of polyethylene glycol concentration in earlywood and latewood. In all the graphs, the progressive numbers displayed in x-axis are used for visualisation purposes only, 0 (%) refers to the untreated sample while only 10–30–50 (%) refers to the real steps of the treatment

consistently show a strong decrease, while the kurtosis parameter (K, in Fig. 8e) increases with increasing polyethylene glycol concentration, indicating a growing deviation from Gaussian diffusion. This highlights the increasing microstructural complexity and restriction experienced by diffusing molecules as PEG accumulates within the wood pore network. The consistency between the trends of D and D_K confirms that both parameters capture the overall reduction of molecular mobility, while the additional increase in K provides sensitivity to microstructural restriction that is not accessible through a single diffusion coefficient alone. Notably, the decrease of D_K and the increase of K are more pronounced in latewood, due to its higher intrinsic microscopic heterogeneity compared to earlywood, if we consider the term "heterogeneity" associated with smaller cell dimensions, thicker cell walls, and a larger solid fraction (Liszka et al. 2023).

3.3 Limitation and reproducibility

The combined analysis of relaxation (T_1, T_2), diffusion (D, D_K), and kurtosis (K) parameters demonstrates that PEG impregnation progressively reduces molecular mobility while increasing diffusion heterogeneity, with distinct responses observed in earlywood and latewood. These results were obtained despite the methodological approximations adopted in the present approach. In particular, a mono-exponential model was used to describe both relaxation and diffusion signal decays, although the strong structural heterogeneity of wood suggests the presence of multiple relaxation and diffusion compartments. The failure to account for multiple compartments is reflected in the increased fitting uncertainties observed for T_1 and D values reported in Table 3. A further limitation arises from the emergence of chemical shift artefacts at elevated PEG concentrations, which indicates the need for further optimisation of the applied imaging protocol. The chemical shift

difference between water and PEG protons (about 1 ppm), leads to signal overlap in diffusion-weighted EPI acquisitions, affecting image resolution and quantitative accuracy. Although these artefacts do not compromise the qualitative trends reported here, they limit the reliability of diffusion metrics at the highest PEG concentrations. Therefore, future improvements, such as the implementation of frequency-selective saturation pulses or selective suppression of water and PEG resonances, are expected to provide greater robustness and precision in identifying different water reservoirs and consolidant distribution within the wood microstructure.

4 Conclusion

In this study, diffusion and relaxation MRI protocols deriving from medical diagnostics research were adapted and applied to the investigation of polyethylene glycol (PEG) impregnation in waterlogged wood. High-resolution µ-MRI enabled non-destructive visualisation of the wood microstructure and the consolidant penetration, with T_2 maps proving particularly useful for visualising the spatial distribution and uneven PEG penetration between earlywood and latewood regions during treatment. Diffusion-weighted imaging provided quantitative insight into molecular mobility within the wood matrix. The mono-exponential diffusion coefficient D was used as a robust and reproducible descriptor of average mobility under the adopted imaging conditions. Deviations from Gaussian diffusion were explicitly addressed through the application of the kurtosis model, with the kurtosis parameter K showing higher sensitivity to increasing microstructural complexity of the wood–solution system than conventional diffusion signal decay alone. In particular, K revealed non-Gaussian diffusion behaviour of multi-compartmentalised water within the complex wood matrix, providing new insights into the confinement effects of the porous structure and the interaction of water-PEG with wood structures.

Building on the results and limitations of this preliminary study, the proposed µ-MRI protocol will be applied to archaeological waterlogged wood, with the aim of non-invasively characterising PEG-water-wood interactions in more complex and degraded systems and supporting the assessment of conservation treatments.

Author contributions Conceptualisation, E.V., V.S., and S.C.; methodology, E.V., A.M., V.S., G.T., and S.C.; formal analysis, E.V. and A.M.; investigation, E.V., S.C., V.S. and G.T.; writing the original draft preparation, E.V.; writing, review and editing, E.V., S.C., A.M., and V.S.; visualisation, E.V and A.M.; supervision, S.C.

Funding Open access funding provided by Università degli Studi di Roma La Sapienza within the CRUI-CARE Agreement.

Data availability The data presented in this study are available on request.

Declarations

Conflict of interest The authors declare no competing interests.

References

Anisimov AV, Sorokina NY, Dautova NR (1998) Water diffusion in biological porous systems: a NMR approach. Magn Reson Imaging 16(5–6):565–568. https://doi.org/10.1016/S0730-725X(98)00053-8

Bannister DA (1990) A pulsed NMR relaxation and diffusion study of water in treated and untreated waterlogged wood. PhD Thesis, University of Nottingham

Bardet M, Gerbaud G, Doan C, Giffard M, Hediger S, De Paëpe G, Trân Q-K (2012) Dynamics property recovery of archaeological-wood fibers treated with polyethylene glycol demonstrated by high-resolution solid-state NMR. Cellulose 19(5):1537–1545. https://doi.org/10.1007/s10570-012-9736-y

Callaghan PT (1991) Principles of nuclear magnetic resonance microscopy. Oxford University Press

Capuani S, Stagno V, Missori M, Sadori L, Longo S (2020) High-resolution multiparametric MRI of contemporary and waterlogged archaeological wood. Magn Reson Chem 58(9):860–869. https://doi.org/10.1002/mrc.5034

Christensen M, Frosch M, Jensen P, Schnell U, Shashoua Y, Nielsen OF (2006) Waterlogged archaeological wood - chemical changes by conservation and degradation. J Raman Spectrosc 37(10):1171–1178. https://doi.org/10.1002/jrs.1589

Christensen M, Kutzke H, Hansen FK (2012) New materials used for the consolidation of archaeological wood-past attempts, present struggles, and future requirements. J Cult Heritage. https://doi.org/10.1016/j.culher.2012.02.013

Clop EM, Perillo MA, Chattah AK (2012) 1H and 2H NMR spin-lattice relaxation probing water: PEG molecular dynamics in solution. J Phys Chem 116(39):11953–11958. https://doi.org/10.1021/jp304569a

Cole-Hamilton DJ, Kaye B, Chudek JA, Hunter G (1995) Nuclear magnetic resonance imaging of waterlogged wood. Stud Conserv 40(1):41. https://doi.org/10.2307/1506610

De Santis S, Rebuzzi M, Di Pietro G, Fasano F, Maraviglia B, Capuani S (2010) In vitro and in vivo MR evaluation of internal gradient to assess trabecular bone density. Phys Med Biol 55(19):5767–5785. https://doi.org/10.1088/0031-9155/55/19/010

De Santis S, Gabrielli A, Palombo M, Maraviglia B, Capuani S (2011) Non-gaussian diffusion imaging: a brief practical review. Magn

Reson Imaging 29(10):1410–1416. https://doi.org/10.1016/j.mri.2011.04.006
Derkaoui N, Said S, Grohens Y, Olier R, Privat M (2007) PEG400 novel phase description in water. J Colloid Interface Sci 305(2):330–338. https://doi.org/10.1016/j.jcis.2006.10.008
Fadnavis S, Chowdhury A, Batson J, Drineas P, Garyfallidis E (2022) Patch2Self denoising of diffusion MRI with self-supervision and matrix sketching. https://doi.org/10.1101/2022.03.15.484539
Gao X, Zhuang S, Jin J, Cao P (2015) Bound water content and pore size distribution in swollen cell walls determined by NMR technology. BioResources. https://doi.org/10.15376/biores.10.4.8208-8224
Han L, Guo J, Tian X, Jiang X, Yin Y (2022) Evaluation of PEG and sugars consolidated fragile waterlogged archaeological wood using nanoindentation and ATR-FTIR imaging. Int Biodeterior Biodegrad 170:105390. https://doi.org/10.1016/j.ibiod.2022.105390
Hoffmann P (1986) On the stabilization of waterlogged Oakwood with PEG. part II. Designing a two-step treatment for multi-quality timbers. Stud Conserv 31(3):103. https://doi.org/10.2307/1506256
Jensen JH, Helpern JA, Ramani A, Lu H, Kaczynski K (2005) Diffusional kurtosis imaging: the quantification of non-gaussian water diffusion by means of magnetic resonance imaging. Magn Reson Med 53(6):1432–1440. https://doi.org/10.1002/mrm.20508
Jora MZ, Cardoso MVC, Sabadini E (2016) Dynamical aspects of water-poly(ethylene glycol) solutions studied by ^{1}H NMR. J Mol Liq 222:94–100. https://doi.org/10.1016/j.molliq.2016.06.101
Kanazawa Y, Yamada T, Kido A, Fujimoto K, Takakura K, Hayashi H, Fushimi Y, Kozawa S, Koizumi K, Okuni M, Ueda N, Togashi K (2017a) Internal evaluation of impregnation treatment of waterlogged wood; relation between concentration of internal materials and relaxation time using magnetic resonance imaging. Magn Reson Imaging 38:196–201. https://doi.org/10.1016/j.mri.2017.01.010
Kanazawa Y, Yamada T, Kido A, Fujimoto K, Takakura K, Hayashi H, Fushimi Y, Kozawa S, Koizumi K, Okuni M, Ueda N, Togashi K (2017b) Visualization of magnetization transfer effect in polyethylene glycol impregnated waterlogged wood. Appl Magn Reson 48(2):125–134. https://doi.org/10.1007/s00723-016-0850-0
Kowalczuk J, Rachocki A, Broda M, Mazela B, Ormondroyd GA, Tritt-Goc J (2019) Conservation process of archaeological waterlogged wood studied by spectroscopy and gradient NMR methods. Wood Sci Technol 53(6):1207–1222. https://doi.org/10.1007/s00226-019-01129-5
Li J, Ma E (2021) Characterization of water in wood by time-domain nuclear magnetic resonance spectroscopy (Td-nmr): a review. Forests. https://doi.org/10.3390/f12070886
Li J, Ma E (2022) 2D time-domain nuclear magnetic resonance (2D TD-NMR) characterization of cell wall water of *fagus sylvatica* and *Pinus taeda* L. Cellulose 29(16):8491–8508. https://doi.org/10.1007/s10570-022-04789-y
Liszka A, Wightman R, Latowski D, Bourdon M, Krogh KBRM, Pietrzykowski M, Lyczakowski JJ (2023) Structural differences of cell walls in earlywood and latewood of *Pinus sylvestris* and their contribution to biomass recalcitrance. Front Plant Sci. https://doi.org/10.3389/fpls.2023.1283093
Lüsse S, Arnold K (1996) The interaction of poly(ethylene glycol) with water studied by ^{1}H and ^{2}H NMR relaxation time measurements. Macromolecules 29(12):4251–4257. https://doi.org/10.1021/ma9508616
Maiuro A, Di Stadio F, Palombo M, Ciardiello A, Satta S, Pernazza A, Leopizzi M, Rocca CD, Catalano C, Manganaro L, Capuani S (2025) Endometrial cancer tissue features clusterization by kurtosis MRI. Med Phys 52(5):2898–2908. https://doi.org/10.1002/mp.17718
Mori M, Kuhara S, Kobayashi K, Suzuki S (2021) Nondestructive visualization of polyethylene glycol impregnation in wood using ultrashort echo time 3D imaging. J Cult Heritage 50:43–48. https://doi.org/10.1016/j.culher.2021.05.008
Nguyen TD, Kohdzuma Y, Endo R, Sugiyama J (2018) Evaluation of chemical treatments on dimensional stabilization of archeological waterlogged hardwoods obtained from the Thang long imperial citadel site, Vietnam. J Wood Sci 64(4):436–443. https://doi.org/10.1007/s10086-018-1719-7
Proietti N, Capitani D, Di Tullio V (2018) Nuclear magnetic resonance, a powerful tool in cultural heritage. Magnetochemistry 4(1):11. https://doi.org/10.3390/magnetochemistry4010011
Rebuzzi M, Vinicola V, Taggi F, Sabatini U, Wehrli FW, Capuani S (2013) Potential diagnostic role of the MRI-derived internal magnetic field gradient in calcaneus cancellous bone for evaluating postmenopausal osteoporosis at 3T. Bone 57(1):155–163. https://doi.org/10.1016/j.bone.2013.07.027
Rehorn C, Blümich B (2018) Cultural heritage studies with mobile NMR. Angew Chem Int Ed 57(25):7304–7312. https://doi.org/10.1002/anie.201713009
Schweingruber FH (2007) Wood Structure and Environment. Springer Berlin Heidelberg. https://doi.org/10.1007/978-3-540-48548-3
Stagno V, Capuani S (2022) Decay of a Roman age pine wood studied by micro magnetic resonance imaging, diffusion nuclear magnetic resonance and portable nuclear magnetic resonance. ACTA IMEKO 11(1):10. https://doi.org/10.21014/acta_imeko.v11i1.1079
Stagno V, Mailhiot S, Capuani S, Galotta G, Telkki VV (2021) Testing 1D and 2D single-sided NMR on Roman age waterlogged woods. J Cult Herit 50:95–105. https://doi.org/10.1016/j.culher.2021.06.001
Stagno V, Moricca C, Sadori L, Dell'Aglio E, Reale R, Capuani S (2023) Evaluation of the efficacy of micro-Magnetic resonance imaging compared with light microscopy to investigate the anatomy of modern and ancient waterlogged wood. Magn Reson Imaging 102:164–178. https://doi.org/10.1016/j.mri.2023.06.011
Stagno V, Mankinen O, Mailhiot S, Telkki V-V, Capuani S (2024) Comprehensive characterization of waterlogged archaeological wood by NMR relaxometry, diffusometry, micro-imaging and cryoporometry. Phys Chem Chem Phys 26(42):27189–27208. https://doi.org/10.1039/D4CP02697G
Stamm AJ (1964) Factors affecting the bulking and dimensional stabilization of wood with polyethylene glycols. For Prod J 19:403–408
Stelzner J, Stelzner I, Martinez-Garcia J, Gwerder D, Wittköpper M, Muskalla W, Cramer A, Heinz G, Egg M, Schuetz P (2022) Stabilisation of waterlogged archaeological wood: the application of structured-light 3D scanning and micro computed tomography for analysing dimensional changes. Heritage Sci 10(1):60. https://doi.org/10.1186/s40494-022-00686-6
Villani E, Popescu CM, Jancelewicz M, Stagno V, Capuani S, Broda M (2025) Sodium alginate as a green consolidant for waterlogged wood—a preliminary study †. Forests. https://doi.org/10.3390/f16020325
Wagner M, Catalano J, Di Tullio V, Pigliapochi R, Zumbulyadis N, Centeno SA, Dybowski C (2023) Applications of NMR spectroscopy in cultural heritage science. Comprehensive Inorganic Chemistry III. Elsevier, pp 788–836. https://doi.org/10.1016/B978-0-12-823144-9.00064-9